Bioorganic & Medicinal Chemistry 19 (2011) 2190–2198

Contents lists available at ScienceDirect

Bioorganic & Medicinal Chemistry

journal homepage: www.elsevier.com/locate/bmc

Radiosynthesis and in vivo evaluation of 1-[^{18}F]fluoroelacridar as a positron emission tomography tracer for P-glycoprotein and breast cancer resistance protein

Bernd Dörner [a,b], Claudia Kuntner [c], Jens P. Bankstahl [d], Thomas Wanek [c], Marion Bankstahl [d], Johann Stanek [b], Julia Müllauer [c], Florian Bauer [a], Severin Mairinger [a,b,c], Wolfgang Löscher [d], Donald W. Miller [e], Peter Chiba [f], Markus Müller [b], Thomas Erker [a,*], Oliver Langer [b,c]

[a] Department of Medicinal Chemistry, University of Vienna, Austria
[b] Department of Clinical Pharmacology, Medical University of Vienna, Austria
[c] Molecular Medicine, AIT Austrian Institute of Technology GmbH, Seibersdorf, Austria
[d] Department of Pharmacology, Toxicology & Pharmacy, University of Veterinary Medicine Hanover, Germany
[e] Department of Pharmacology and Therapeutics, University of Manitoba, Winnipeg, Manitoba, Canada
[f] Institute of Medical Chemistry, Medical University of Vienna, Austria

ARTICLE INFO

Article history:
Received 11 December 2010
Revised 18 February 2011
Accepted 19 February 2011
Available online 26 February 2011

Keywords:
PET
1-[^{18}F]Fluoroelacridar
P-glycoprotein
Breast cancer resistance protein
Blood–brain barrier

ABSTRACT

Aim of this study was to label the potent dual P-glycoprotein (Pgp) and breast cancer resistance protein (BCRP) inhibitor elacridar (**1**) with ^{18}F to provide a positron emission tomography (PET) radiotracer to visualize Pgp and BCRP. A series of new 1- and 2-halogen- and nitro-substituted derivatives of **1** (**4a–e**) was synthesized as precursor molecules and reference compounds for radiolabelling and shown to display comparable in vitro potency to **1** in increasing rhodamine 123 accumulation in a cell line overexpressing human Pgp (MDCKII-MDR1). 1-[^{18}F]fluoroelacridar ([^{18}F]**4b**) was synthesized in a decay-corrected radiochemical yield of 1.7 ± 0.9% by a 1-step no-carrier added nucleophilic aromatic ^{18}F-substitution of 1-nitro precursor **4c**. Small-animal PET imaging of [^{18}F]**4b** was performed in naïve rats, before and after administration of unlabelled **1** (5 mg/kg, n = 3), as well as in wild-type and *Mdr1a/b*$^{(-/-)}$*Bcrp1*$^{(-/-)}$ mice (n = 3). In PET experiments in rats, administration of unlabelled **1** increased brain activity uptake by a factor of 9.5 (p = 0.0002, 2-tailed Student's t-test), whereas blood activity levels remained unchanged. In *Mdr1a/b*$^{(-/-)}$*Bcrp1*$^{(-/-)}$ mice, the mean brain-to-blood ratio of activity at 60 min after tracer injection was 7.6 times higher as compared to wild-type animals (p = 0.0002). HPLC analysis of rat brain tissue extracts collected at 40 min after injection of [^{18}F]**4b** revealed that 93 ± 7% of total radioactivity in brain was in the form of unchanged [^{18}F]**4b**. In conclusion, the in vivo behavior of [^{18}F]**4b** was found to be similar to previously described [^{11}C]**1** suggesting transport of [^{18}F]**4b** by Pgp and/or BCRP at the rodent BBB. However, low radiochemical yields and a significant degree of in vivo defluorination will limit the utility of [^{18}F]**4b** as a PET tracer.

1. Introduction

The adenosine triphosphate (ATP) binding cassette (ABC) transporters P-glycoprotein (Pgp,[†] ABCB1) and breast cancer resistance protein (BCRP, ABCG2) act as gatekeepers at the level of the vascular endothelium of the blood–brain barrier (BBB) preventing brain uptake of a wide range of lipophilic molecules by active ATP-driven efflux transport.[1] Changes in ABC transporter function and expression are believed to be involved in several neurological disorders, such as therapy refractory epilepsy, Parkinson's and Alzheimer's disease.[1]

Visualization of ABC transporters with the non-invasive nuclear imaging method positron emission tomography (PET) might help to better understand disease related changes in transporter function/expression.[2] Two classes of radiotracers for visualization of Pgp have been described so far. Radiolabelled Pgp substrates such as (*R*)-[^{11}C]verapamil[3] or [^{11}C]-*N*-desmethyl-loperamide[4] and radiolabelled Pgp inhibitors such as [^{11}C]laniquidar,[5] [^{11}C]elacridar,[6,7] [^{11}C]tariquidar[8,9] and [^{11}C]MC18[10] (Fig. 1). Radiolabelled Pgp inhibitors were initially developed to provide PET tracers

* Corresponding author. Tel.: +43 1 4277 550 03; fax: +43 1 4277 9 551.
E-mail addresses: thomas.erker@univie.ac.at (T. Erker), oliver.langer@ait.ac.at (O. Langer).

[†] *Abbreviations:* BBB, blood–brain barrier; BCRP, breast cancer resistance protein; IC_{50}, half-maximum inhibitory concentration; MDCKII-MDR1, Madin-Darby canine kidney epithelial cells stably transfected with the human MDR1 gene; *Mdr1a/b*$^{(-/-)}$ *Bcrp1*$^{(-/-)}$ mouse, Pgp/Bcrp1 knockout mouse; PET, positron emission tomography; Pgp, P-glycoprotein; R123, rhodamine 123; SPE, solid-phase extraction; SUV, standardized uptake value; TAC, time-activity curve.

0968-0896/$ - see front matter © 2011 Elsevier Ltd. All rights reserved.
doi:10.1016/j.bmc.2011.02.039

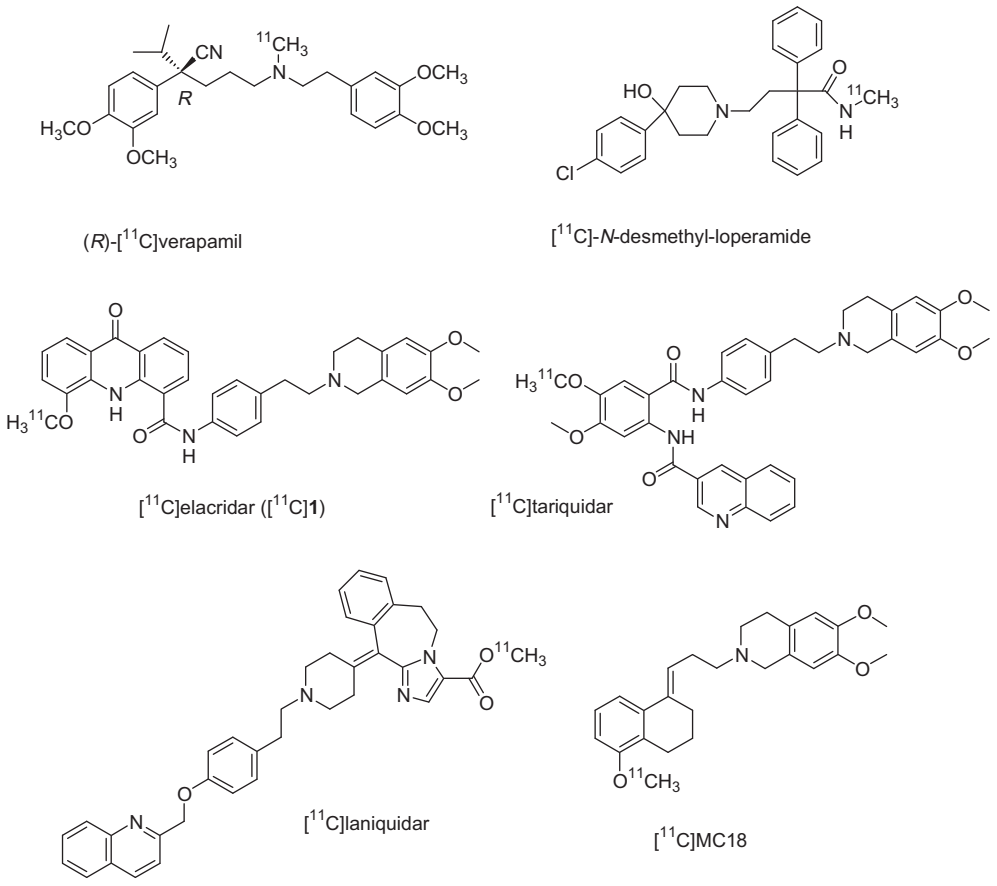

Figure 1. Chemical structures of Pgp substrate and inhibitor PET tracers.

which should bind to Pgp without being transported and therefore allow for visualization of Pgp expression levels as opposed to substrates which visualize Pgp function. However, the in vivo behavior of most radiolabelled Pgp inhibitors tested to date in rodents was found to be 'substrate-like' in that brain activity uptake in baseline scans was equally low or even lower than for radiolabelled substrates and several times increased after administration of unlabelled inhibitor. Our recent experiments with [^{11}C]elacridar ([^{11}C]**1**, Fig. 1) in rats and transporter knockout and wild-type mice suggested that this radiotracer was efficiently transported by Pgp and/or BCRP at the rodent BBB.[6] Given its favorable metabolic profile with radiometabolites not being taken up into brain tissue, [^{11}C]**1**[6,7] appeared as an interesting candidate probe to investigate Pgp and BCRP. Due to the short radioactive half-life of ^{11}C (20.4 min) the use of ^{11}C-labelled PET tracers is restricted to centers with an onsite cyclotron. In order to facilitate a broader applicability of this radiotracer we aimed at labelling **1** with the longer-lived radionuclide ^{18}F (half-life: 109.8 min).

Here we report on the synthesis of a series of new halogen- and nitro-substituted derivatives of **1**, which we found to possess comparable potency to **1** in inhibiting Pgp transport in vitro. Moreover, we report on the radiosynthesis and small-animal PET evaluation of 1-[^{18}F]fluoroelacridar ([^{18}F]**4b**), which we showed to display similar in vivo behavior as [^{11}C]**1**.

2. Results

2.1. Chemistry and radiolabelling

The *para*- and the *meta*-position relative to the carboxylamide group in the acridone moiety of **1** were selected for no-carrier-added nucleophilic aromatic substitution with [^{18}F]F$^-$. 1-Fluoroelacridar (**4b**) and 2-fluoroelacridar (**4e**) were synthesized as shown in Scheme 1.[6,11] As radiolabelling precursors, 1- and 2-chloro substituted derivatives **4a** and **4d** as well as 1-nitro derivative **4c** were synthesized according to Scheme 1.[6,11] In small-scale experiments precursor molecules **4a**, **4c** and **4d** were reacted with the K[^{18}F]F–K_{222} complex using different solvents (DMF, DMSO), different reaction temperatures (120–180 °C) and different reaction times (5–60 min). Derivatives **4a** and **4d** failed to provide any ^{18}F-incorporation under all conditions tested, whereas **4c** gave the corresponding 1-[^{18}F]fluoro-derivative [^{18}F]**4b** in an incorporation yield of 10–20% based on radio-thin layer chromatography (radio-TLC) analysis of crude reaction mixture. The synthesis of [^{18}F]**4b** was automated in a TRACERlab FX synthesis module. [^{18}F]**4b**, ready for intravenous (iv) injection, was obtained in a decay-corrected radiochemical yield of 1.7 ± 0.9% (n = 7) based on [^{18}F]F$^-$ in a total synthesis time of 147 min. Radiochemical purity was greater than 98% and the specific activity at the end of synthesis was 8 ± 4 GBq/μmol (n = 7). The identity of [^{18}F]**4b** was confirmed by high-performance liquid chromatography (HPLC) coinjection with unlabelled reference compound **4b**.

2.2. Assessment of Pgp inhibitory activity

Pgp inhibition of compounds **4a**–**e** was determined relative to reference compound **1** using the rhodamine 123 (R123) accumulation assay in a cell line which overexpressed human Pgp (MDCKII-MDR1) (Table 1). Four compounds displayed comparable potency to **1** in inhibiting R123 efflux with half-maximum inhibitory concentrations (IC_{50}) in the 0.5–2 μM range (**4b**–**e**). For instance, 1-fluoro-derivative **4b**, which was also tested in vivo in ^{18}F-labelled form (see below), had an only about four times higher IC_{50} than **1**. It is noteworthy that all derivatives were less effective

Table 1
Effects of compound **1** and the new modulators **4a–e** on R123 efflux from MDCKII-MDR1 cell monolayers

Compound	IC_{50} (μM)	log IC_{50}[a]	Maximal inhibitory effect[b] (%)
1 (elacridar)	0.4	−0.36 ± 0.06	100
4a	3.8	0.58 ± 0.04	74 ± 3
4b	1.7	0.24 ± 0.04	81 ± 4
4c	1.6	0.21 ± 0.07	50 ± 4
4d	1.4	0.14 ± 0.08	88 ± 5
4e	0.6	−0.21 ± 0.08	69 ± 1

[a] log IC_{50} values (fitted parameter ± standard error) were estimated using GraphPad Prism software.
[b] Maximal inhibitory effects (%) are expressed as inhibition caused by the highest concentration of the compound tested (**4b**, **4d**, **4e**: 10 μM; **4a**, **4c**: 100 μM) relative to the inhibitory effect caused by 3.2 μM **1** (100% inhibition).

than **1** in terms of increasing intracellular R123 concentration in MDCKII-MDR1 cells with maximal inhibitory effects relative to **1** <100% (Table 1).

2.3. Small-animal PET in rats and mice

[^{18}F]**4b** was evaluated in two groups of rats. The first group underwent a 150 min PET scan, during which unlabelled **1** was iv administered at a dose of 5 mg/kg at 60 min after injection of [^{18}F]**4b**. The second group of rats was scanned at 2 h after administration of **1**. In the first group of rats, brain uptake of activity was low before unlabelled **1** was administered (Fig. 2A). Peak brain uptake was 0.46 ± 0.12 (standardized uptake value, SUV) at

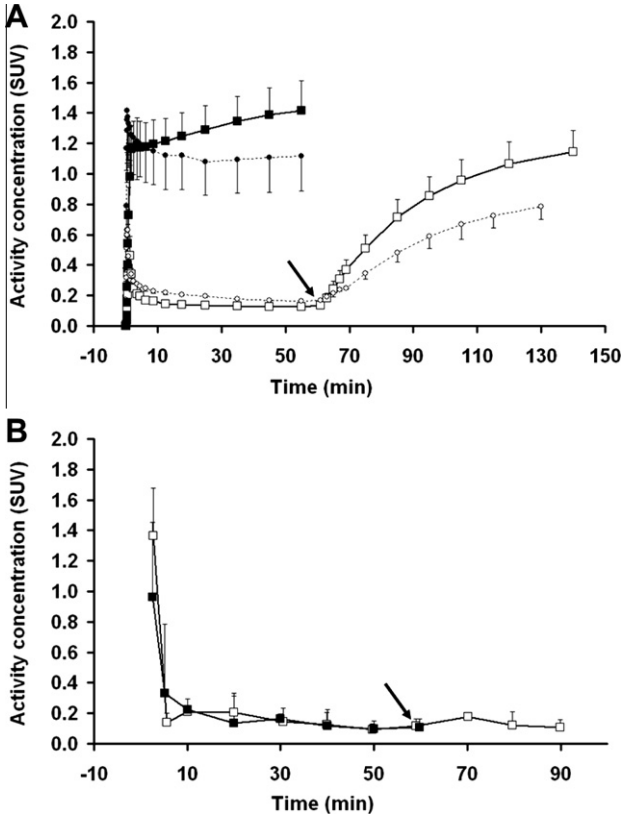

Figure 2. TACs (mean SUV ± SD) of [^{18}F]**4b** in whole brain (A) and arterial blood (B) of rats (group 1: open squares, group 2: filled squares). In group 1, unlabelled **1** was administered as an iv bolus over 60 s at 60 min after injection of [^{18}F]**4b**. The time point of administration of **1** is indicated by an arrow. Group 2 was scanned at 2 h after administration of **1**. For comparison, whole-brain TACs (mean SUV ± SD, n = 3) previously obtained with [^{11}C]**1**[6] are also shown in A (group 1: open circles, group 2: filled circles).

0.9–1.3 min after tracer injection. At 25 min after tracer injection, brain activity uptake had declined to 0.14 ± 0.02 SUV. In response to administration of unlabelled **1** at 60 min after injection of [^{18}F]**4b** there was a steep increase in brain activity concentration, reaching a SUV of 1.14 ± 0.14 at 140 min after tracer injection (Fig. 2A), whereas blood activity levels remained unchanged (Fig. 2B). In group 2, which was scanned at 2 h after administration of unlabelled **1**, brain activity uptake at 25 min after tracer injection was 9.5 times higher (p = 0.0002) as compared to group 1 (Fig. 2A) with similar blood activity levels as in group 1 (Fig. 2B). In Figure 3, representative PET summation images are shown for scans recorded before and after inhibitor administration. There was appreciable uptake of radioactivity in bone tissue which pointed to in vivo defluorination of [^{18}F]**4b** (Fig. 3). In the first group of rats, activity uptake in humerus was 1.42 ± 0.37 and 4.59 ± 1.00 SUV at 1.8 and 140 min after injection of [^{18}F]**4b**, respectively.

Radiometabolites of [^{18}F]**4b** in plasma were assessed in a separate group of rats (n = 3) by a solid-phase extraction (SPE) assay. At 10, 20, 30 and 40 min after injection of [^{18}F]**4b** into rats, 6 ± 4%, 6 ± 3%, 12 ± 5% and 13 ± 4% of total plasma activity was recovered in SPE fractions 1 and 2 (corresponding to polar radiometabolites of [^{18}F]**4b**) and 94 ± 4%, 94 ± 3%, 88 ± 5% and 87 ± 4% in fraction 3 (corresponding to unchanged [^{18}F]**4b** and its lipophilic radiometabolites). Fraction 3 from the 40 min sample was further analyzed by HPLC, which showed that 72 ± 27% of total radioactivity was in the form of unchanged [^{18}F]**4b**, whereas the remainder of radioactivity eluted before [^{18}F]**4b** on reversed-phase HPLC. [^{18}F]**4b** was 98.0 ± 1.7% (n = 3) protein-bound in rat plasma. Brain extracts collected at 40 min after injection of [^{18}F]**4b** into rats were also analyzed by HPLC showing that 93 ± 7% of total radioactivity in brain was in the form of unchanged [^{18}F]**4b**.

In Figure 4, PET summation images and brain time-activity curves (TACs) of [^{18}F]**4b** in wild-type and *Mdr1a/b*$^{(-/-)}$*Bcrp1*$^{(-/-)}$ mice are shown. Brain TACs were several times higher in *Mdr1a/b*$^{(-/-)}$*Bcrp1*$^{(-/-)}$ mice as compared to wild-type animals (Fig. 4B). Brain activity uptake at 60 min after tracer injection was normalized to blood activity levels measured after the PET scan. The mean brain-to-blood ratio of activity at 60 min after tracer injection was 7.6 times higher (p = 0.0002) in *Mdr1a/b*$^{(-/-)}$*Bcrp1*$^{(-/-)}$ mice than in wild-type animals (brain-to-blood ratios, wild-type: 1.5 ± 0.2; *Mdr1a/b*$^{(-/-)}$*Bcrp1*$^{(-/-)}$: 11.6 ± 1.4).

3. Discussion

The aim of this study was to label the potent dual Pgp/BCRP inhibitor **1** with the positron emitting radionuclide ^{18}F in order to develop a longer-lived PET radiotracer, based on **1**, than previously described [^{11}C]**1**[6,7] to investigate Pgp and BCRP in vivo. During the preparation of this manuscript a study by Kawamura et al. has appeared in the literature, which also reported the synthesis of an ^{18}F-derivative of **1** (i.e., the corresponding 5-[^{18}F]fluoroethoxy derivative), but this radiotracer was labelled in a different position than in our work.[12] We found that the acridone moiety of **1** gave straightforward access to the introduction of appropriate leaving groups (Cl, NO_2) in the 1- and 2-positions for ^{18}F-substitution (Scheme 1). Derivatives **4a–e** were prepared as reference compounds and radiolabelling precursors for ^{18}F-fluorination of **1** (Scheme 1). As **4a–e** are previously unknown close structural analogues of **1** they were tested for their Pgp inhibitory potencies in the R123 accumulation assay (Table 1). All compounds except for 1-chloro-derivative **4a** were remarkably potent in the Pgp inhibition assay with IC_{50} values in the 0.5–2.0 μM range, which was comparable to **1** (IC_{50}: 0.4 μM). As the primary imaging target was Pgp, BCRP modulation of derivatives **4a–e** was not tested.

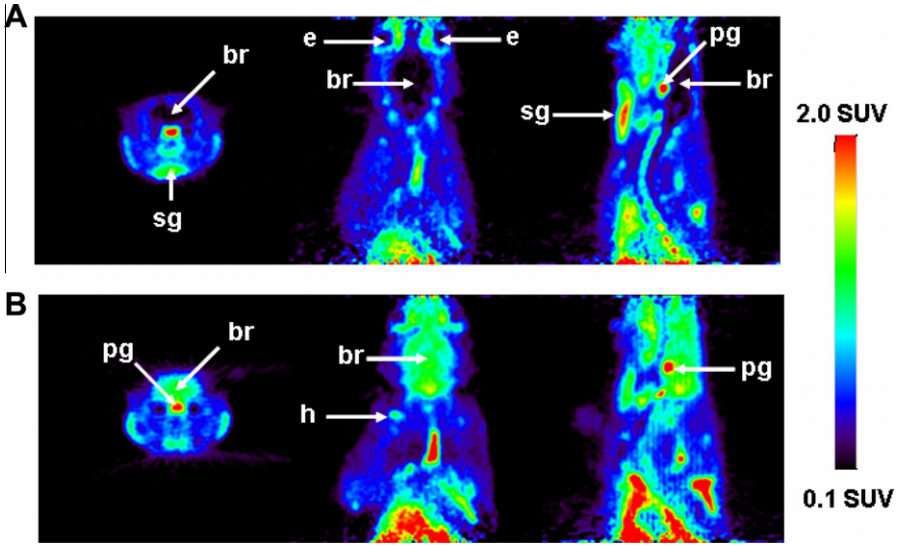

Figure 3. Exemplary coronal (left), horizontal (center) and sagittal (right) PET summation images in rats, (A) before (group 1: 0–60 min) and (B) after administration of unlabelled **1** (5 mg/kg). The radiation scale is set from 0.1 to 2.0 SUV. Anatomical structures are indicated by arrows (br, brain; e, eye; h, humerus; sg, submandibular gland; pg, pituitary gland).

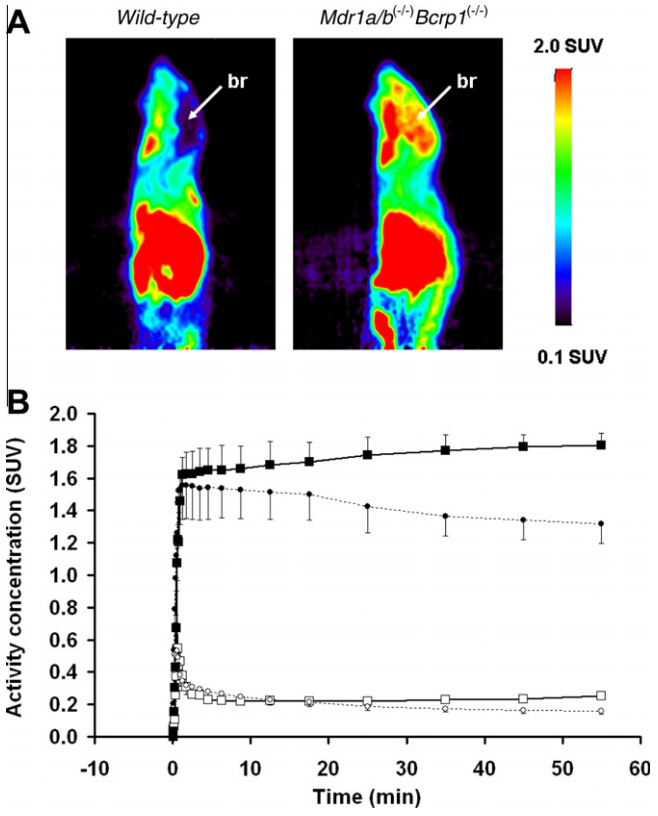

Figure 4. (A) Sagittal PET summation images (0–60 min) of [^{18}F]**4b** in wild-type and *Mdr1a/b*$^{(-/-)}$*Bcrp1*$^{(-/-)}$ mice. The radiation scale is set from 0.1 to 2.0 SUV. Anatomical structures are indicated by arrows (br, brain). (B) TACs (mean SUV ± SD, $n = 3$ per mouse type) of [^{18}F]**4b** in whole brain of wild-type (open squares), and *Mdr1a/b*$^{(-/-)}$*Bcrp1*$^{(-/-)}$ mice (filled squares). For comparison TACs (mean SUV ± SD, $n = 3$) previously obtained with [^{11}C]**1**[24] are also shown (wild-type mice: open circles, *Mdr1a/b*$^{(-/-)}$*Bcrp1*$^{(-/-)}$ mice: filled circles).

Radiolabelling experiments revealed that only the 1-position of the acridone moiety was moderately activated for ^{18}F-substitution. 1-[^{18}F]fluoroelacridar ([^{18}F]**4b**) was synthesized in low radiochemical yield of 1.7 ± 0.9% based on starting [^{18}F]F$^-$ employing rather drastic reaction conditions (60 min heating at 175 °C) (Scheme 1). Surprisingly, the specific activity of [^{18}F]**4b** at end of synthesis (8 ± 4 GBq/μmol) was lower than expected for a typical no-carrier added nucleophilic aromatic ^{18}F-substitution reaction (>37 GBq/μmol). The most likely explanation for the low specific activity of [^{18}F]**4b** was that elimination of the NO_2 group in precursor molecule **4c** had occurred under the employed labelling conditions giving rise to unlabelled **1**, which we failed to separate from **4b** on all tested HPLC systems. The obtained amounts of [^{18}F]**4b** were sufficiently high to allow for conducting small-animal PET experiments.

The primary aim of the PET examination was to assess if in vivo [^{18}F]**4b** behaved similarly to previously developed [^{11}C]**1**. Therefore we chose a similar study set-up as we had previously used for [^{11}C]**1**, which was studied in naïve rats by performing paired PET scans before and after administration of unlabelled **1**.[6] However, due to the longer half-life of ^{18}F it was not possible to perform paired PET scans in the same animals with [^{18}F]**4b** and therefore separate groups of rats were examined. As previously observed for [^{11}C]**1**[6] the in vivo behavior of [^{18}F]**4b** was consistent with that of a transported substrate (Fig. 2A). Brain activity uptake of [^{18}F]**4b** was low in the first group of rats, which was scanned before administration of unlabelled **1**. In response to administration of **1** there was a steep increase in brain activity uptake (Fig. 2A). In the second group of rats, which was scanned after administration of **1**, brain activity uptake was 9.5 times higher as compared to group 1. It seems unlikely that the rather low specific activity of [^{18}F]**4b** should have significantly affected the PET results. Kawamura and co-workers have previously studied uptake of [^{11}C]**1** into mouse brain in the presence of increasing amounts of unlabelled **1** (0.1–10 mg/kg, iv) and found that brain uptake of [^{11}C]**1** started to increase at doses greater than 0.1 mg/kg with a half-maximum effect dose of 1.55 mg/kg.[7] As the doses of unlabelled carrier administered in our in vivo experiments in rats and mice were <0.05 mg/kg the relatively low specific activity of [^{18}F]**4b** should not have influenced its brain uptake. As a second approach to the rat studies, in which Pgp/BCRP was pharmacologically inhibited with unlabelled **1**, we performed PET experiments with [^{18}F]**4b** in wild-type and in transporter knockout mice, which lacked both Pgp and Bcrp1. Absence of Pgp/Bcrp1 at the BBB was reflected by a 7.6 times higher brain-to-blood ratio of activity as compared to wild-type mice. Overall, the in vivo behavior of [^{18}F]**4b** was almost

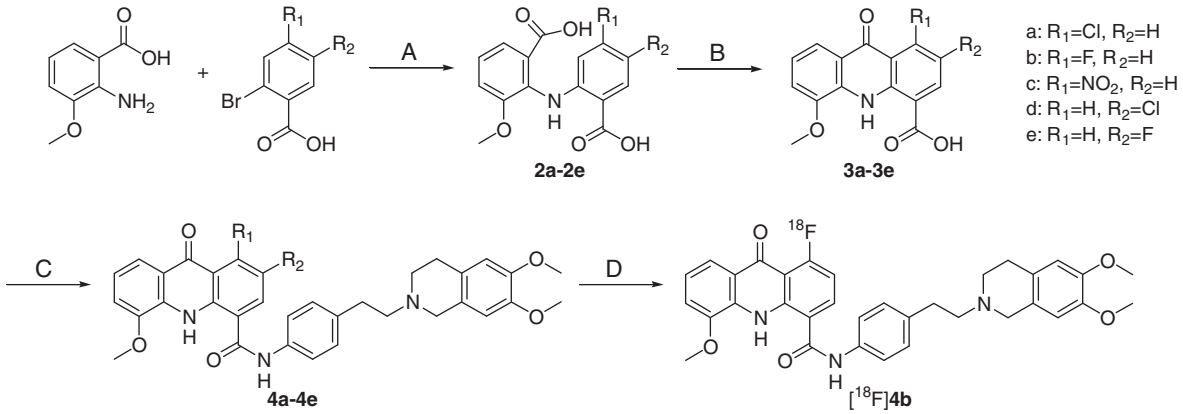

Scheme 1. Synthesis of nitro- and halogen-substituted derivatives of **1** (**4a–e**) and ^{18}F-labelling of **4c** to give [^{18}F]**4b**. Reagents and conditions: (A) Cu^0/K_2CO_3, EtOH, reflux; (B) $POCl_3$, CH_3CN, reflux; (C) TBTU, Et_3N, DMF, rt; (D) K[^{18}F]F-K_{222}, DMSO, 175 °C.

identical to that of [^{11}C]**1** as reflected by quite similar TACs of both radiotracers in rats and mice (Figs. 2A and 4).

Our in vivo results obtained with [^{18}F]**4b** are to a certain extent surprising as **1** has been previously characterized as a non-transported inhibitor of Pgp. It has been shown that **1** does not stimulate adenosine triphosphatase (ATPase) activity and has an efflux ratio that is <2 in cell monolayer transport assays, consistent with a lack of Pgp transport activity.[13,14] However, very recent data suggest that the structurally related Pgp inhibitor tariquidar (Fig. 1), which we have also labelled with ^{11}C and which was shown to behave similarly to [^{11}C]**1** and [^{18}F]**4b** in vivo,[8] is an avid substrate of BCRP.[15] Kannan et al. found that accumulation of ^{3}H-labelled tariquidar (1 nM) was several fold-lower in a cell line overexpressing human BCRP relative to the parental cell line and increased to similar levels as in parental cells after co-incubation with the BCRP inhibitor fumitremorgin C, which was consistent with BCRP transport of tariquidar.[15] On the other hand, when a cell line which overexpressed human Pgp, was incubated with [^{3}H]tariquidar, cellular uptake was higher relative to parental cells, which pointed to binding of [^{3}H]tariquidar to Pgp. In addition, recent PET results obtained with [^{11}C]tariquidar and [^{11}C]**1** in *Mdr1a/b*$^{(-/-)}$, *Bcrp1*$^{(-/-)}$ and *Mdr1a/b*$^{(-/-)}$*Bcrp1*$^{(-/-)}$ mice suggest that the two radiotracers are transported by Bcrp1 and possibly Pgp at the murine BBB.[7,8] Given the close structural similarity between **1** and tariquidar and the similar in vivo behavior of [^{11}C]**1** and [^{18}F]**4b** on one hand and [^{11}C]tariquidar on the other hand it seems very likely that the 'substrate-like' behavior of [^{18}F]**4b** was caused by BCRP and possibly Pgp transport. This is also in good agreement with the observation that pharmacological doses of **1**, which are known to inhibit BCRP and Pgp transport at the BBB,[16] significantly increased brain uptake of [^{18}F]**4b** in rats. As no radiotracers have been described to date to measure BCRP transport in vivo it definitely appears worthwhile to further characterize PET tracers based on **1** and tariquidar with respect to such a future application. Moreover, dual Pgp/BCRP substrate radiotracers could help to better understand the interplay of these two transporters at the BBB. This class of radiotracers appears particularly attractive as it has been shown that they lack brain uptake of radiometabolites[7,9] which has been found to be a considerable limitation of the Pgp substrate probes (*R*)-[^{11}C]verapamil[17] and [^{11}C]-*N*-desmethyl-loperamide.[18] In line with previous results obtained with [^{11}C]**1**[6,7] and [^{11}C]tariquidar,[8,9] we could show that >90% of total activity in rat brain was due to unchanged [^{18}F]**4b**. However, a considerable drawback of [^{18}F]**4b** was the significant degree of in vivo defluorination observed during the time course of the PET experiments as reflected by the high amount of radioactivity in bone tissue which would hamper the quantification of [^{18}F]**4b** uptake in organs with low uptake which are surrounded by bone structures.

4. Material and methods

4.1. General

Unless otherwise stated, all chemicals were purchased from Sigma-Aldrich Chemie GmbH (Schnelldorf, Germany), TCI Europe (Zwijndrecht, Belgium), Merck (Darmstadt, Germany) or Apollo Scientific Ltd (Bredbury, UK) at analytical grade and used without further purification. Isoflurane was obtained from Baxter Vertriebs GmbH (Vienna, Austria). The hydrochloride salt of **1** was obtained from Glaxo SmithKline (Research Triangle Park, NC, USA). For administration **1** hydrochloride was dissolved freshly on each experimental day in a 20% aqueous (aq) EtOH solution and injected at a volume of 2 mL/kg. Aqueous [^{18}F]F$^-$ was produced in a General Electrics PETtrace cyclotron (General Electric Healthcare, Uppsala, Sweden) via the ^{18}O(*p*,*n*)^{18}F nuclear reaction by irradiation of a 2 mL water target containing 95.9% enriched [^{18}O]H_2O (Hyox18, Rotem Industries, Beer Sheva, Israel) with 16.5 MeV proton beam. Typical irradiation times were 60 min with a beam current of 40 μA, which yielded a [^{18}F]F$^-$ amount of about 110 GBq at end of bombardment. ^{1}H and ^{13}C NMR spectra were recorded on a Bruker Advance DPx200 (200 and 50 MHz). Chemical shifts are reported in δ units (ppm) relative to Me_4Si line as internal standard (s, br s, d, m, Cq for singlet, broad singlet, doublet, multiplet and quaternary carbon, respectively) and *J* values are reported in Hertz. Mass spectra (MS) were obtained with a Shimadzu (GC-17A; MS-QP5050A) spectrometer. Purity of the intermediates **2a–e** and **3a–e** was established by combustion analysis with a Perkin-Elmer 2400 CHN elemental analyzer and of the key compounds **4a–e** by analytical HPLC confirming a purity >95%.

4.2. General synthesis procedure for compounds 2a–e

A suspension of 2-amino-3-methoxybenzoic acid (1.67 g, 10 mmol), 2-bromobenzoic acid derivative (11 mmol, 1.1 equiv), K_2CO_3 (2.77 g, 20 mmol, 2 equiv) and copper powder (0.125 g, 2 mmol, 0.2 equiv) was stirred in EtOH (20 mL) and heated to reflux for 1.5 h. The suspension was cooled to room temperature and H_2O (20 mL) was added. The mixture was filtered on cellite to remove the copper. The filter bed was washed with H_2O and the resulting solution was acidified with concentrated HCl to a

pH of 2–3. The resulting suspension was stirred for 1 h at 10 °C, the solid was filtered and washed with H_2O. The product was recrystallized in EtOH/H_2O and dried under vacuum.

4.2.1. 2-((2-Carboxy-5-chlorophenyl)amino)-3-methoxybenzoic acid (2a)

The compound was synthesized according to the general procedure using 2-bromo-4-chlorobenzoic acid (2.59 g, 11 mmol, 1.1 equiv) as 2-bromobenzoic acid derivative. Yield: 2.95 g (92%) white crystals. Mp: 250–251 °C. MS *m/z*: 323 (23%, M^+, ^{37}Cl), 321 (62%, M^+, ^{35}Cl), 258 (100%), 230 (74%), 74 (58%). ^1H NMR (DMSO-d_6) δ 3.79 (s, 3H, OCH_3), 6.27 (s, 1H), 6.77 (d, 1H, J = 8.4 Hz), 7.27–7.44 (m, 2H), 7.45–7.55 (m, 1H), 7.85 (d, 1H, J = 8.4 Hz), 10.08 (s, 1H), 13.17 (br s, 2H). ^{13}C NMR (DMSO-d_6) δ 55.7 (OCH_3), 111.4 (Cq), 113.6 (CH), 115.8 (CH), 116.7 (CH), 122.3 (CH), 125.4 (CH), 127.0 (Cq), 128.0 (Cq), 132.8 (CH), 138.1 (Cq), 148.1 (Cq), 153.6 (Cq), 167.7 (COOH), 168.6 (COOH).

4.2.2. 2-((2-Carboxy-5-fluorophenyl)amino)-3-methoxybenzoic acid (2b)

The compound was synthesized according to the general procedure with 2-bromo-4-fluorobenzoic acid (2.41 g, 11 mmol, 1.1 equiv) as 2-bromobenzoic acid derivative. Yield: 3.00 g (98%) pale white crystals. Mp: 206–209 °C. MS *m/z*: 305 (49%, M^+), 242 (83%), 213 (100%), 184 (35%), 93 (47%). ^1H NMR (DMSO-d_6) δ 3.78 (s, 3H, OCH_3), 5.94–6.03 (m, 1H), 6.46–6.60 (m, 1H), 7.27–7.39 (m, 2H), 7.40–7.49 (m, 1H), 7.84–7.96 (m, 1H), 10.11 (s, 1H), 13.04 (br s, 2H). ^{13}C NMR (DMSO-d_6) δ 55.7 (OCH_3), 100.1 (d, CH, J = 25.9 Hz), 104.0 (d, CH, J = 22.2 Hz), 109.2 (Cq), 115.7 (CH), 122.2 (CH), 125.4 (CH), 127.1 (Cq), 127.9 (Cq), 133.8 (d, CH, J = 11.5), 149.6 (d, Cq, J = 12.2), 153.6 (Cq), 165.4 (d, CF, J = 246.1 Hz), 167.7 (COOH), 168.6 (COOH).

4.2.3. 2-((2-Carboxy-5-nitrophenyl)amino)-3-methoxybenzoic acid (2c)

The compound was synthesized according to the general procedure with 2-bromo-4-nitrobenzoic acid (2.71 g, 11 mmol, 1.1 equiv) as 2-bromobenzoic acid derivative. Yield: 3.19 g (96%) orange crystals. Mp: 279–284 °C. MS *m/z*: 332 (67%, M^+), 269 (67%), 89 (66%), 75 (100%), 51 (75%). ^1H NMR (DMSO-d_6) δ 3.78 (s, 3H, OCH_3), 7.02–7.07 (m, 1H), 7.28–7.47 (m, 2H), 7.48–7.57 (m, 2H), 8.08 (d, 1H, J = 8.8 Hz), 10.35 (br s, 1H), 13.43 (br s, 2H). ^{13}C NMR (DMSO-d_6) δ 55.8 (OCH_3), 109.2 (CH), 110.6 (CH), 116.0 (CH), 117.6 (Cq), 122.6 (CH), 125.5 (CH), 126.3 (Cq), 127.8 (Cq), 132.6 (CH), 147.1 (Cq), 150.2 (Cq), 153.2 (Cq), 167.7 (COOH), 168.0 (COOH).

4.2.4. 2-((2-Carboxy-4-chlorophenyl)amino)-3-methoxybenzoic acid (2d)

The compound was synthesized according to the general procedure using 2-bromo-5-chlorobenzoic acid (2.57 g, 11 mmol) as 2-bromobenzoic acid derivative.[19] Yield: 2.80 g (87%) ochre crystals. Mp: 225–229 °C. MS *m/z*: 323 (24%, M^+, ^{37}Cl), 321 (63%, M^+, ^{35}Cl), 260 (35%), 258 (100%), 230 (68%), 44 (85%). ^1H NMR (DMSO-d_6): δ 3.75 (s, 3H, OCH_3), 6.35 (d, 1H, J = 9 Hz), 7.15–7.39 (m, 3H), 7.40–7.52 (m, 1H), 7.75–7.79 (m, 1H), 10.16 (br s, 1H), 12.97 (br s, 2H). ^{13}C NMR (DMSO-d_6): δ 55.6 (OCH_3), 113.9 (Cq), 115.6 (CH), 116.7 (CH), 120.0 (Cq), 122.2 (CH), 124.7 (CH), 126.4 (Cq), 128.6 (Cq), 129.7 (CH), 132.7 (CH), 145.7 (Cq), 153.4 (Cq), 167.8 (COOH), 168.0 (COOH).

4.2.5. 2-((2-Carboxy-4-fluorophenyl)amino)-3-methoxybenzoic acid (2e)

The compound was synthesized according to the general procedure with 2-bromo-5-fluorobenzoic acid (2.41 g, 11 mmol) as 2-bromobenzoic acid derivative.[19] Yield: 2.84 g (93%) light yellow crystals. Mp: 209–214 °C. MS *m/z*: 305 (58%, M^+), 242 (100%), 214 (95%), 83 (35%), 57 (53%). ^1H NMR (DMSO-d_6): δ 3.74 (s, 3H, OCH_3), 6.30–6.41 (m, 1H), 7.10–7.35 (m, 3H), 7.42–7.59 (m, 2H), 9.93 (br s, 1H), 13.12 (br s, 2H). ^{13}C NMR (DMSO-d_6): δ 55.5 (OCH_3), 113.3 (d, Cq, J = 6.4 Hz), 115.6 (CH), 115.7 (d, CH, J = 22.8 Hz), 116.5 (d, CH, J = 7.3 Hz), 120.4 (d, CH, J = 22.8 Hz), 122.3 (CH), 124.1 (CH), 125.7 (Cq), 129.5 (Cq), 143.4 (d, Cq), J = 1.3 Hz), 153.3 (Cq), 153.6 (d, Cq, J = 232.5 Hz), 167.9 (COOH), 168.1 (d, COOH, J = 2.5 Hz).

4.3. General synthesis procedure for compounds 3a–e

Compounds **2a–e** (5 mmol) were dissolved in CH_3CN (15 mL) and heated to reflux. Phosphorus(V)oxychloride (1 mL, 11 mmol, 2.2 equiv) was added over a period of 1 h. The solution was refluxed for further 2 h and then cooled to 10–15 °C. H_2O (10 mL) was added and the mixture heated to reflux for additional 2.5 h. The suspension was cooled to 10 °C and filtered. The solid was washed with H_2O and CH_3CN and then dried under vacuum.

4.3.1. 1-Chloro-5-methoxyacridone-4-carboxylic acid (3a)

Cyclization of compound **2a** (1.61 g, 5 mmol) yielding the title compound was carried out using the general approach. Yield: 1.12 g (73%) green solid. Mp: 315–320 °C. MS *m/z*: 305 (25%, M^+, ^{37}Cl), 303 (75%, M^+, ^{35}Cl), 257 (66%), 151 (88%), 62 (100%). ^1H NMR (DMSO-d_6) δ 4.03 (s, 3H, OCH_3), 7.13–7.36 (m, 3H), 7.67 (d, 1H, J = 8.2 Hz), 8.24 (d, 1H, J = 8.2 Hz), 12.5 (s, 1H). ^{13}C NMR (DMSO-d_6) δ 56.5 (OCH_3), 112.9 (CH), 113.5 (Cq), 116.9 (CH), 117.3 (Cq), 122.1 (CH), 122.1 (Cq), 123.1 (CH), 129.6 (Cq), 136.0 (CH), 139.6 (Cq), 142.8 (Cq), 147.2 (Cq), 168.8 (COOH), 175.4 (CO).

4.3.2. 1-Fluoro-5-methoxyacridone-4-carboxylic acid (3b)

Cyclization of compound **2b** (1.53 g, 5 mmol) to **3b** was carried out using the general approach. Yield: 1.16 g (81%) green/brown solid. Mp: 275–278 °C. MS *m/z*: 287 (100%, M^+), 269 (74%), 254 (67%), 241 (71%), 170 (37%). ^1H NMR (DMSO-d_6) δ 4.03 (s, 3H, OCH_3), 6.92–7.07 (m, 1H), 7.15–7.28 (m, 1H), 7.34 (d, 1H, J = 7.8 Hz), 7.67 (d, 1H, J = 7.8 Hz), 8.31–8.42 (m, 1H), 12.39 (s, 1H). ^{13}C NMR (DMSO-d_6) δ 56.5 (OCH_3), 107.0 (d, CH, J = 21.6 Hz), 110.7 (d, Cq, J = 9.0 Hz), 110.7 (d, Cq, J = 4.2 Hz), 113.0 (CH), 116.6 (CH), 122.1 (Cq), 138.2 (d, CH, J = 13.2 Hz), 142.9 (d, Cq, J = 5.2 Hz), 147.3 (Cq), 165.0 (d, CF, J = 268.6 Hz), 168.6 (COOH), 174.8 (d, CO, J = 1.7 Hz).

4.3.3. 5-Methoxy-1-nitroacridone-4-carboxylic acid (3c)

Cyclization of compound **2c** (1.66 g, 5 mmol) yielding the title compound was carried out using the general approach. Yield: 1.29 g (82%) brown solid. Mp: 284–290 °C. MS *m/z*: 314 (31%, M^+), 313 (34%), 121 (47%), 57 (100%), 51 (55%). ^1H NMR (DMSO-d_6) δ 4.02 (s, 3H, OCH_3), 7.19–7.41 (m, 2H), 7.51 (d, 1H, J = 8.0 Hz), 7.64 (d, 1H, J = 7.8 Hz), 8.50 (d, 1H, J = 8.0 Hz), 12.49 (s, 1H). ^{13}C NMR (DMSO-d_6) δ 56.5 (OCH_3), 111.2 (Cq), 113.5 (CH), 114.1 (CH), 116.5 (CH), 117.3 (Cq), 121.0 (Cq), 122.7 (CH), 130.1 (Cq), 137.2 (CH), 141.1 (Cq), 147.4 (Cq), 151.6 (Cq), 167.9 (COOH), 173.4 (CO).

4.3.4. 2-Chloro-5-methoxyacridone-4-carboxylic acid (3d)

Cyclization of compound **2d** (1.61 g, 5 mmol) to **3d** was carried out using the general approach.[19] Yield: 1.21 g (79%) dark green solid. Mp: 309–314 °C. MS *m/z*: 305 (35%, M^+, ^{37}Cl), 303 (100%, M^+, ^{35}Cl), 285 (85%), 270 (52%), 257 (76%). ^1H NMR (DMSO-d_6): δ 4.05 (s, 3H, OCH_3), 7.19–7.43 (m, 2H), 7.69–7.77 (m, 1H), 8.25–8.38 (m, 2H), 12.07 (s, NH). ^{13}C NMR (DMSO-d_6): δ 56.5 (OCH_3), 113.2 (CH), 116.8 (CH), 117.3 (Cq), 120.7 (Cq), 122.1 (CH), 122.6 (Cq), 124.5 (Cq), 130.6 (Cq), 130.7 (CH), 135.7 (CH), 138.8 (Cq), 147.4 (Cq), 167.8 (COOH), 175.1 (CO).

4.3.5. 2-Fluoro-5-methoxyacridone-4-carboxylic acid (3e)

Cyclization of compound **2e** (1.53 g, 5 mmol) yielding the title compound was carried out using the general approach.[19] Yield: 1.22 g (85%) ochre solid. Mp: >350 °C. MS *m/z*: 287 (100%, M^+), 269 (58%), 254 (63%), 241 (67%), 92 (51%). ^{1}H NMR (DMSO-d_6): δ 4.05 (s, 3H, OCH_3), 7.18–7.41 (m, 2H), 7.68–7.77 (m, 1H), 8.08–8.23 (m, 2H), 12.04 (s, NH). ^{13}C NMR (DMSO-d_6): δ 56.5 (OCH_3), 112.9 (CH), 116.6 (d, CH, J = 22.5 Hz), 116.7 (CH), 117.3 (d, Cq, J = 6.5 Hz), 120.0 (Cq), 121.8 (CH), 122.5 (d, Cq, J = 6.0 Hz), 124.1 (d, CH, J = 25.7 Hz), 130.7 (Cq), 137.1 (Cq), 147.3 (Cq), 155.3 (d, CF, J = 239.0 Hz), 167.8 (d, COOH, J = 2.3 Hz), 175.4 (d, CO, J = 2.6 Hz).

4.4. General synthesis procedure for key compounds 4a–e

To a solution of 6,7-dimethoxy-2-(4-aminophenethyl)-1,2,3,4-tetrahydroisochinoline (0.312 g, 1 mmol), which has been prepared as described elsewhere,[6] and compound **3a**–**e** (1 mmol, 1 equiv) in DMF (2 mL) *O*-(benzotriazol-1-yl)-*N*,*N*,*N*′,*N*′-tetramethyluronium hexafluorophosphate (HBTU, 0.379 g, 1.05 mmol, 1.05 equiv) and Et_3N (0.29 mL, 2.1 mmol, 2.1 equiv) were added. The solution was stirred for 2 h at rt, and then a mixture of H_2O and isopropyl alcohol (1/1, v/v, 2 mL) was added. The mixture was stirred for additional 30 min. The obtained slurry was filtered, washed with MeOH and H_2O, and dried under vacuum.

4.4.1. 1-Chloro-*N*-(4-(2-(6,7-dimethoxy-1,2,3,4-tetrahydroisoquinolin-2-yl)ethyl)phenyl)-5-methoxyacridone-4-carboxamide (1-chloroelacridar, 4a)

The compound was synthesized according to the general procedure with **3a** (0.304 g, 1 mmol) as reactant. Yield: 0.335 g (56%) ochre solid. Mp: 183–189 °C. HRMS (ESI/MS) calcd for $C_{34}H_{32}O_5N_3ClH$: 598.2109, found: 598.2102. ^{1}H NMR (DMSO-d_6) δ 2.69–2.91 (m, 8H, 4 × CH_2), 3.58 (s, 2H, CH_2), 3.70 (s, 6H, 2 × OCH_3), 4.02 (s, 3H, OCH_3), 6.61–6.69 (m, 2H), 7.17–7.43 (m, 5H), 7.64 (d, 2H, J = 8.0 Hz), 7.74 (d, 1H, J = 8.0 Hz), 8.31 (d, 1H, J = 8.0 Hz), 10.63 (s, 1H), 12.66 (s, 1H).

4.4.2. *N*-(4-(2-(6,7-Dimethoxy-1,2,3,4-tetrahydroisoquinolin-2-yl)ethyl)phenyl)-1-fluoro-5-methoxyacridone-4-carboxamide (1-fluoroelacridar, 4b)

Starting from **3b** (0.287 g, 1 mmol) the title compound was synthesized according to the general approach. Yield: 0.337 g (58%) brown solid. Mp: 215–220 °C. HRMS (ESI/MS) calcd for $C_{34}H_{32}O_5N_3FH$: 582.2404, found: 582.2414. ^{1}H NMR (DMSO-d_6) δ 2.63–3.10 (m, 8H, 4 × CH_2), 3.65 (s, 2H, CH_2), 3.69 (s, 6H, 2 × OCH_3), 6.59–6.73 (m, 2H), 7.02–7.22 (m, 2H), 7.24–7.35 (m, 3H), 7.58–7.75 (m, 3H), 8.36–8.52 (m, 1H), 10.58 (s, 1H), 12.65 (s, 1H).

4.4.3. *N*-(4-(2-(6,7-Dimethoxy-1,2,3,4-tetrahydroisoquinolin-2-yl)ethyl)phenyl)-5-methoxy-1-nitroacridone-4-carboxamide (1-nitroelacridar, 4c)

According to the general procedure the compound was synthesized using **3c** (0.314 g, 1 mmol, 1 equiv) as reactant. Yield: 0.305 g (50%) brown solid. Mp: 167–172 °C. HRMS (ESI/MS) calcd for $C_{34}H_{32}O_7N_4H$: 609.2349, found: 609.2355. ^{1}H NMR (DMSO-d_6) δ 2.70–3.04 (m, 8H, 4 × CH_2), 3.67–3.83 (m, 8H, CH_2, 2 × OCH_3), 4.05 (s, 3H, OCH_3), 6.65–6.75 (m, 2H), 7.25–7.44 (m, 4H), 7.56–7.84 (m, 4H), 8.52–8.63 (m, 1H), 10.81 (br s, 1H), 12.61 (br s, 1H).

4.4.4. 2-Chloro-*N*-(4-(2-(6,7-dimethoxy-1,2,3,4-tetrahydroisoquinolin-2-yl)ethyl)phenyl)-5-methoxyacridone-4-carboxamide (2-chloroelacridar, 4d)

The title compound was synthesized using the general approach starting from **3d** (0.304 g, 1 mmol) as reactant. Yield: 0.353 g (59%) yellow solid. Mp: 188–195 °C. HRMS (ESI/MS) calcd for $C_{34}H_{32}O_5N_3ClH$: 598.2109, found: 598.2105. ^{1}H NMR ($CDCl_3$) δ 2.72–3.02 (m, 8H, 4 × CH_2), 3.67 (s, 2H, CH_2), 3.85 (s, 6H, 2 × OCH_3), 4.06 (s, 3H, OCH_3), 6.56 (s, 1H), 6.61 (s, 1H), 7.08–7.32 (m, 4H), 7.63–7.76 (m, 2H), 7.95–8.13 (m, 1H), 8.31 (d, 1H, J = 2.2 Hz), 8.60 (d, 1H, J = 2.2 Hz), 9.92 (s, 1H), 12.25 (s, 1H).

4.4.5. *N*-(4-(2-(6,7-Dimethoxy-1,2,3,4-tetrahydroisoquinolin-2-yl)ethyl)phenyl)-2-fluoro-5-methoxyacridone-4-carboxamide (2-fluoroelacridar, 4e)

Starting from **3e** (0.287 g, 1 mmol) the title compound was synthesized according to the general procedure. Yield: 0.399 g (69%) dark-orange solid. Mp: 152–157 °C. HRMS (ESI/MS) calcd for $C_{34}H_{32}O_5N_3FH$: 582.2404, found 582.2398. ^{1}H NMR (DMSO-d_6) δ 2.56–2.96 (m, 8H, 4 × CH_2), 3.57 (s, 2H, CH_2), 3.70 (s, 6H, 2 × OCH_3), 4.03 (s, 3H, OCH_3), 6.60–6.69 (m, 2H), 7.16–7.40 (m, 4H), 7.61–7.73 (m, 2H), 7.73–7.80 (m, 1H), 8.10–8.18 (m, 1H), 8.38–8.47 (m, 1H), 10.63 (s, 1H), 12.26 (s, 1H).

4.5. General procedure for small-scale [^{18}F]fluorination of compounds 4a, 4c and 4d

Aqueous [^{18}F]F^- ion from the cyclotron target was collected into a 3 mL Wheaton V-vial (Wheaton Science Products, Millville, USA) containing a solution of kryptofix 2.2.2 in CH_3CN (120 mg/mL, 100–200 μL; 12.0–24.0 mg, 32.7–65.4 μmol) and a solution of K_2CO_3 in H_2O (200 mg/mL, 20–40 μL; 4.0–8.0 mg, 28.9–57.8 μmol). The mixture was exposed to a stream of argon and concentrated to dryness at 130 °C under repeated addition of CH_3CN (3 × 0.5 mL). To the dried K[^{18}F]F–K_{222} complex, the respective precursor (**4a**, **4c**, **4d**: 3–12 μmol) dissolved in dry DMSO or DMF (0.5 mL each) was added and the resulting solution stirred for 5–60 min at 120–180 °C. An aliquot of the reaction mixture was analyzed by TLC. For TLC analysis Merck Silica Gel 60 F_{254} plates were used with ethyl acetate/MeOH 2:1 (v/v) as mobile phase. TLC plates were analyzed using a phosphor imager (Cyclone, Packard Instruments, Meriden, CN, USA). Retardation factors (R_f): [^{18}F]F^-: 0.0; [^{18}F]**4b**: 0.6–0.7.

4.6. 1-[^{18}F]Fluoroelacridar ([^{18}F]4b)

The synthesis of [^{18}F]**4b** was automated in a TRACERlab FX synthesis module (General Electric Healthcare). After delivery of the irradiated [^{18}O]H_2O to the synthesis module, [^{18}F]F^- was trapped on a Chromafix 30-PS-HCO_3 ion exchange cartridge, which had been pre-activated with EtOH (2 mL) and H_2O (2 mL). [^{18}F]F^- was eluted to the synthesis reactor by rinsing the cartridge with a mixture of kryptofix 2.2.2. (24 mg, 63.8 μmol) in CH_3CN (0.9 mL) and K_2CO_3 (3.5 mg, 57.1 μmol) in H_2O (0.1 mL). The solvent was evaporated under vacuum for 5 min at 75 °C, then CH_3CN (1 mL) was added and the mixture heated under vacuum for 5 min at 130 °C to remove the remaining H_2O. To the dried K[^{18}F]F–K_{222} complex, radiolabelling precursor **4c** (6 mg, 9.9 μmol) dissolved in dry DMSO (1 mL) was added and the reaction mixture heated for 60 min at 175 °C. The reaction mixture was then cooled to 40 °C, diluted with a mixture of CH_3CN and 0.1% aq trifluoroacetic acid (TFA) (1:1, v/v, 3 mL) and injected into the built-in HPLC system. A Hamilton-PRP1 column (500 × 8 mm, 10 μm) was eluted at a flow rate of 4 mL/min with a gradient (0–20 min) from CH_3CN/0.1% aq TFA 35:65 (v/v) to 45:55. The HPLC eluate was monitored in series for ultraviolet (UV) absorption at a wavelength of 257 nm and radioactivity. On this system radiolabelling precursor **4c** and product [^{18}F]**4b** eluted with retention times of 23 and 19–20 min, respectively. The product fraction was diluted with H_2O (100 mL) and passed over a C18 Sep-Pak Plus cartridge (Waters cooperation, Milford, MA), which had been pre-activated with EtOH (5 mL) and H_2O (10 mL). The

cartridge was then washed with H_2O (10 mL), followed by elution of [^{18}F]**4b** with EtOH (3 mL). The EtOH was removed by heating at 90 °C under a stream of argon and the product formulated in a mixture of 5 mg sodium ascorbate in 0.9% aq NaCl solution/EtOH/polyethylene glycol 300 (50:15:35, v/v/v) for iv injection into animals. Radiochemical and chemical purity and specific activity of [^{18}F]**4b** were determined by analytical radio-HPLC using a Hamilton-PRP1 column (290 × 4 mm, 10 μm) eluted at a flow rate of 1 mL/min using a gradient (0–25 min) from CH_3CN/0.1% aq TFA 35:65 (v/v) to 45:55. UV detection was performed at a wavelength of 257 nm. The retention time of [^{18}F]**4b** was 16–18 min on this HPLC system.

4.7. Cell line and culture condition

Madin-Darby canine kidney epithelial cells stably transfected with the human MDR1 gene (MDCKII-MDR1), which were obtained from the National Cancer Institute (Bethesda, MD, USA), were used for the fluorescent screening studies. Cells were cultured in Dulbecco's Modified Eagles medium (DMEM) supplemented with 80 ng/mL colchicine to maintain high expression of Pgp as previously described.[20] Cells were seeded onto 24-well culture plates at a density of 65,000 cells/cm^2 and used for functional assays upon reaching confluency (typically 3 days).

4.8. Assessment of Pgp inhibitory activity

Pgp inhibition of derivatives **4a–e** was determined as previously described.[21] Briefly, confluent MDCKII-MDR1 monolayers were pretreated with pH 7.4 Tyrodes balanced salt solution (TBSS): 136 mM NaCl, 1.8 mM $CaCl_2$, 1 mM $MgCl_2$, 0.36 mM NaH_2PO_4, 5.56 mM D-glucose and 5 mM HEPES. Various concentrations of **4a–e** (**4b**, **4d**, **4e**: 0.1–10 μM; **4a**, **4c**: 0.1–100 μM, n = 3 per concentration) were added to the TBSS and the cells were incubated for 30 min at 37 °C. Following the preincubation period, the TBSS was removed and replaced with fresh TBSS containing 3.2 μM R123 to assess drug efflux transporter activity. Cellular accumulation of the fluorescent dye was monitored over a 60 min period, under control conditions and in the presence of various concentrations of **4a–e** (see above). After this time, cells were washed three times with ice-cold phosphate buffered saline solution and the cells were solubilized in 1.0% Triton-X100 (0.5 mL). Aliquots (100 μL) of the solubilized cell solutions were removed for determination of intracellular R123 accumulation using a Synergy HT fluorescent plate reader. Protein content was determined using the Pierce BCA method and the data were expressed as the amount of fluorescent probe (nmol) per mg cell protein. Concentration response curves were fitted using GraphPad Prism 5 software (GraphPad Software, Inc., San Diego, CA, USA) and compared to maximal inhibition achieved using **1** at a concentration of 3.2 μM.

4.9. Animals

Adult female Sprague–Dawley rats weighing 260–300 g were obtained from Harlan Netherlands (Horst, Netherlands). Female FVB (wild-type) and *Mdr1a/b*$^{(-/-)}$*Bcrp1*$^{(-/-)}$ mice weighing 27–35 g were purchased from Taconic Inc. (Germantown, USA). Prior to each experiment, the animals were placed into an induction box and anesthetized with 2.5% isoflurane. When unconscious, the animals were taken from the box and kept under anesthesia with 1.5–2% isoflurane administered via a mask during the whole experiment. The animals were warmed throughout the whole experiment at around 38 °C. Rats were implanted with catheters into the femoral artery (for blood sampling) and vein (for administration of [^{18}F]**4b** and **1**). In mice, a lateral tail vein was used for radiotracer administration. The study was approved by the local Animal Welfare Committee and all study procedures were performed in accordance with the Austrian Animal Experiments Act.

4.10. Small-animal PET imaging and PET data analysis

The anesthetized animals were positioned in the imaging chamber of the microPET Focus220 scanner (Siemens, Medical Solutions, Knoxville, USA). Animals were injected with [^{18}F]**4b** (rats: 33 ± 3 MBq (mean ± standard deviation, SD) in a volume of about 0.3 mL corresponding to 9.6 ± 6.5 nmol or 20 ± 12 μg/kg body weight unlabelled **4b**; mice: 6 ± 1 MBq in a volume of about 0.1 mL corresponding to 2.0 ± 1.1 nmol or 39 ± 22 μg/kg unlabelled **4b**) as an iv bolus over approximately 40 s. At the start of radiotracer injection, dynamic PET imaging was initiated.

Two groups of rats were scanned with [^{18}F]**4b** (n = 3 per group). One group underwent a 150 min PET scan with [^{18}F]**4b** during which **1** (5 mg/kg) was administered iv over approximately 60 s at 60 min after injection of [^{18}F]**4b**. The other group underwent a 60 min PET scan at 2 h after injection of **1**. During experiments in rats, 5-μL arterial blood samples were withdrawn manually with pre-weighted micropipettes from the femoral artery (approximately every 5 s) during the first 3 min after radiotracer injection, followed by further 10-μL samples taken at 5, 10, 20, 30, 40, 50, 60, 70, 80 and 90 min (last three time points for group 1 only). Mice (n = 3 per mouse type) underwent single 60-min PET scans with [^{18}F]**4b**. At the end of the PET scan, venous blood was withdrawn from mice by retro-orbital puncture into pre-weighted micropipettes. Blood samples from rats and mice were weighted and counted for activity in a 1-detector Wallac gamma counter (Perkin Elmer Instruments, Wellesley, USA), which had been cross-calibrated with the PET camera. Blood activity data were corrected for radioactive decay and corrected for injected dose per gram body weight and expressed as SUV.

PET images were reconstructed by Fourier rebinning followed by 2-dimensional filtered back projection with a ramp filter. The standard data correction protocol (normalization, attenuation, decay correction and injection decay correction) was applied to the data. Whole brain and humerus (in rats) were manually outlined on multiple planes of the PET summation images using the image analysis software Amide and TACs, expressed as SUV, were calculated. For the mouse data, the SUV values measured with PET in brain tissue of individual animals during the last time frame (50–60 min after radiotracer injection) were divided by the SUV value measured in whole blood at the end of the PET scan to obtain brain-to-blood ratios of activity. For all outcome parameters, differences between groups were tested with a 2-tailed Student's t-test. The level of statistical significance was set to p <0.05.

4.11. Metabolism and plasma protein binding of [^{18}F]4b

A group of three rats was injected with [^{18}F]**4b** (74 ± 23 MBq in a volume of about 0.3 mL corresponding to 17.2 ± 3.9 nmol or 37 ± 10 μg/kg body weight unlabelled **4b**) without performing PET examination in order to assess metabolism of [^{18}F]**4b**. At 10, 20 and 30 min after radiotracer injection 0.5 mL blood samples were collected into heparinized vials. At 40 min after radiotracer injection rats were sacrificed, their brains removed and a terminal blood sample (5 mL) collected. Plasma collected at all time points was centrifuged (3000g, 5 min, 21 °C) and analyzed for radiometabolites of [^{18}F]**4b** using a previously described SPE assay.[22] In brief, arterial plasma was spiked with a solution of unlabelled **4b** in DMSO (1 mg/mL, 10 μL) and acidified with 5 M aq. HCl (40 μL) and loaded on a Sep-Pak vac tC18 cartridge (Waters Corporation, Milford, USA), which had been pre-activated with MeOH (3 mL) and H_2O (5 mL). The cartridge was first washed with H_2O (5 mL) and then eluted with MeOH (4 mL). Radioactivity in all three

fractions (plasma, H_2O, MeOH) was measured in the 1-detector Wallac gamma counter. For the 40 min blood sample, the MeOH fraction was 1:1 diluted with 0.1% aq TFA and analyzed by HPLC (injected volume: 2 mL). A Chromolith Performance RP 18-e (100–4.6 mm) column was eluted at flow rate of 5 mL/min using a gradient (0–20 min) from CH_3CN/0.1% aq TFA 20:80 (v/v) to 25/75. UV detection was performed at a wavelength of 257 nm. The retention time of [^{18}F]**4b** was 13–15 min on this HPLC system. For validation of the SPE assay, [^{18}F]**4b** dissolved in mouse plasma (0.5 mL) was subjected to the SPE procedure showing that all radioactivity was quantitatively recovered in the MeOH fraction.

Rat brain was washed twice with ice-cold H_2O and homogenized in 0.9% aq. NaCl solution (0.8 mL) using an IKA T10 basic Ultra-turrax (IKA Laboratory Equipment, Staufen, Germany). The brain homogenate was mixed with CH_3CN (1.5 mL) and centrifuged (3 min, 4 °C, 13,000*g*). The supernatant was diluted 1:1 with 0.1% aq TFA and injected into the same HPLC system used for analysis of radiometabolites in plasma (injected volume: 2 mL). Plasma protein binding of [^{18}F]**4b** was determined by incubating fresh plasma samples obtained from naïve rats with [^{18}F]**4b** during 30 min at 37 °C, followed by ultrafiltration using Amicon Microcon YM-10 centrifugal filter devices (Millipore Corporation, USA) as described previously.[23]

5. Conclusions

In an attempt to label the potent dual Pgp/BCRP inhibitor **1** with ^{18}F we synthesized a series of new 1- and 2-halogen- and nitro-substituted derivatives of **1**, which were found to display comparable potency to **1** in inhibiting Pgp transport of R123 in MDCKII-MDR1 cells. The 1-[^{18}F]fluoro derivative of **1** ([^{18}F]**4b**) was synthesized in moderate radiochemical yield and characterized in rats and mice with small-animal PET. [^{18}F]**4b** was found to display comparable in vivo behavior to previously described [^{11}C]**1** in that brain activity uptake was low in baseline scans and several times increased after administration of unlabelled **1**, suggesting that [^{18}F]**4b** is efficiently transported by BCRP and/or Pgp and at the rodent BBB. However, the significant degree of in vivo defluorination observed with [^{18}F]**4b** together with low radiochemical yields will in all likelihood limit its future utility as a PET tracer.

Acknowledgments

The research leading to these results has received funding from the European Community's Seventh Framework Programme (FP7/2007-2013) under grant agreement number 201380 ('Euripides') and from the Austrian Science Fund (FWF) project 'Transmembrane Transporters in Health and Disease' (SFB F35). The authors thank Michael Sauberer (AIT), Thomas Filip and Maria Zsebedics (Seibersdorf Laboratories GmbH) for their skilful help with laboratory animal handling and the staff of the radiochemistry laboratory (Seibersdorf Laboratories GmbH) for continuous support. **1** hydrochloride was kindly provided by Glaxo SmithKline (Research Triangle Park, NC, USA).

References and notes

1. Löscher, W.; Potschka, H. *Prog. Neurobiol.* **2005**, *76*, 22.
2. Kannan, P.; John, C.; Zoghbi, S. S.; Halldin, C.; Gottesman, M. M.; Innis, R. B.; Hall, M. D. *Clin. Pharmacol. Ther.* **2009**, *86*, 368.
3. Luurtsema, G.; Molthoff, C. F.; Windhorst, A. D.; Smit, J. W.; Keizer, H.; Boellaard, R.; Lammertsma, A. A.; Franssen, E. J. *Nucl. Med. Biol.* **2003**, *30*, 747.
4. Lazarova, N.; Zoghbi, S. S.; Hong, J.; Seneca, N.; Tuan, E.; Gladding, R. L.; Liow, J. S.; Taku, A.; Innis, R. B.; Pike, V. W. *J. Med. Chem.* **2008**, *51*, 6034.
5. Luurtsema, G.; Schuit, R. C.; Klok, R. P.; Verbeek, J.; Leysen, J. E.; Lammertsma, A. A.; Windhorst, A. D. *Nucl. Med. Biol.* **2009**, *36*, 643.
6. Dörner, B.; Kuntner, C.; Bankstahl, J. P.; Bankstahl, M.; Stanek, J.; Wanek, T.; Stundner, G.; Mairinger, S.; Löscher, W.; Müller, M.; Langer, O.; Erker, T. *J. Med. Chem.* **2009**, *52*, 6073.
7. Kawamura, K.; Yamasaki, T.; Konno, F.; Yui, J.; Hatori, A.; Yanamoto, K.; Wakizaka, H.; Takei, M.; Kimura, Y.; Fukumura, T.; Zhang, M. R. *Mol. Imaging Biol.* **2011**, *13*, 152.
8. Bauer, F.; Kuntner, C.; Bankstahl, J. P.; Wanek, T.; Bankstahl, M.; Stanek, J.; Mairinger, S.; Dörner, B.; Löscher, W.; Müller, M.; Erker, T.; Langer, O. *Bioorg. Med. Chem.* **2010**, *18*, 5489.
9. Kawamura, K.; Konno, F.; Yui, J.; Yamasaki, T.; Hatori, A.; Yanamoto, K.; Wakizaka, H.; Takei, M.; Nengaki, N.; Fukumura, T.; Zhang, M. R. *Ann. Nucl. Med.* **2010**, *24*, 403.
10. van Waarde, A.; Ramakrishnan, N. K.; Rybczynska, A. A.; Elsinga, P. H.; Berardi, F.; de Jong, J. R.; Kwizera, C.; Perrone, R.; Cantore, M.; Sijbesma, J. W. A.; Dierckx, R. A.; Colabufo, N. A. *J. Med. Chem.* **2009**, *52*, 4524.
11. Sharp, M. J.; Mader, C. J.; Strachan, C. PCT Int. Appl. WO 98/52923 A1, 1998.
12. Kawamura, K.; Yamasaki, T.; Konno, F.; Yui, J.; Hatori, A.; Yanamoto, K.; Wakizaka, H.; Ogawa, M.; Yoshida, Y.; Nengaki, N.; Fukumura, T.; Zhang, M. R. *Bioorg. Med. Chem.* **2011**, *19*, 861.
13. Colabufo, N. A.; Berardi, F.; Cantore, M.; Perrone, M. G.; Contino, M.; Inglese, C.; Niso, M.; Perrone, R.; Azzariti, A.; Simone, G. M.; Porcelli, L.; Paradiso, A. *Bioorg. Med. Chem.* **2008**, *16*, 362.
14. Polli, J. W.; Wring, S. A.; Humphreys, J. E.; Huang, L.; Morgan, J. B.; Webster, L. O.; Serabjit-Singh, C. S. *J. Pharmacol. Exp. Ther.* **2001**, *299*, 620.
15. Kannan, P.; Telu, S.; Shukla, S.; Ambudkar, S. V.; Pike, V. W.; Halldin, C.; Gottesman, M. M.; Innis, R. B.; Hall, M. D. *ACS Chem. Neurosci.* **2011**, *2*, 82.
16. Agarwal, S.; Sane, R.; Ohlfest, J. R.; Elmquist, W. F. *J. Pharmacol. Exp. Ther.* **2011**, *336*, 223.
17. Luurtsema, G.; Molthoff, C. F.; Schuit, R. C.; Windhorst, A. D.; Lammertsma, A. A.; Franssen, E. J. *Nucl. Med. Biol.* **2005**, *32*, 87.
18. Seneca, N.; Zoghbi, S. S.; Shetty, H. U.; Tuan, E.; Kannan, P.; Taku, A.; Innis, R. B.; Pike, V. W. *Nucl. Med. Biol.* **2010**, *37*, 335.
19. Stankiewicz-Drogon, A.; Dörner, B.; Erker, T.; Boguszewska-Chachulska, A. M. *J. Med. Chem.* **2010**, *53*, 3117.
20. Bachmeier, C. J.; Trickler, W. J.; Miller, D. W. *Drug Metab. Dispos.* **2006**, *34*, 998.
21. Bachmeier, C. J.; Miller, D. W. *Pharm. Res.* **2005**, *22*, 113.
22. Mairinger, S.; Langer, O.; Kuntner, C.; Wanek, T.; Bankstahl, J. P.; Bankstahl, M.; Stanek, J.; Dörner, B.; Bauer, F.; Baumgartner, C.; Löscher, W.; Erker, T.; Müller, M. *Nucl. Med. Biol.* **2010**, *37*, 637.
23. Kuntner, C.; Bankstahl, J. P.; Bankstahl, M.; Stanek, J.; Wanek, T.; Stundner, G.; Karch, R.; Brauner, R.; Meier, M.; Ding, X. Q.; Müller, M.; Löscher, W.; Langer, O. *Eur. J. Nucl. Med. Mol. Imaging* **2010**, *37*, 942.
24. Kuntner, C.; Bankstahl, J. P.; Bankstahl, M.; Stanek, J.; Wanek, T.; Dörner, B.; Bauer, F.; Mairinger, S.; Erker, T.; Müller, M.; Löscher, W.; Langer, O. *Neuroimage* **2010**, *52*, S25. symposium abstract.